



**HAL**  
open science

## Dissociative electron recombination of $\text{NH}_2\text{CHOH}^+$ and implications for interstellar formamide abundance

Mehdi Ayouz, C. Yuen, N. Balucani, C. Ceccarelli, I Schneider, V. Kokoouline

► **To cite this version:**

Mehdi Ayouz, C. Yuen, N. Balucani, C. Ceccarelli, I Schneider, et al.. Dissociative electron recombination of  $\text{NH}_2\text{CHOH}^+$  and implications for interstellar formamide abundance. *Monthly Notices of the Royal Astronomical Society*, 2019, 490 (1), pp.1325-1331. 10.1093/mnras/stz2658 . hal-02569494

**HAL Id: hal-02569494**

**<https://centralesupelec.hal.science/hal-02569494>**

Submitted on 22 May 2023

**HAL** is a multi-disciplinary open access archive for the deposit and dissemination of scientific research documents, whether they are published or not. The documents may come from teaching and research institutions in France or abroad, or from public or private research centers.

L'archive ouverte pluridisciplinaire **HAL**, est destinée au dépôt et à la diffusion de documents scientifiques de niveau recherche, publiés ou non, émanant des établissements d'enseignement et de recherche français ou étrangers, des laboratoires publics ou privés.

# Dissociative electron recombination of $\text{NH}_2\text{CHOH}^+$ and implications for interstellar formamide abundance

M. A. Ayouz,<sup>1</sup> C. H. Yuen,<sup>2</sup> N. Balucani<sup>3,4</sup>, C. Ceccarelli,<sup>4</sup> I. F. Schneider<sup>5,6</sup> and V. Kokoouline<sup>2</sup>★

<sup>1</sup>LGPM, CentraleSupélec, Université Paris-Saclay, 8-10 Rue Joliot Curie, F-91190 Gif-sur-Yvette, France

<sup>2</sup>Department of Physics, University of Central Florida, Orlando, FL 32816, USA

<sup>3</sup>Dipartimento di Chimica, Biologia e Biotecnologie, Università di Perugia, Via Elce di Sotto 8, I-06123 Perugia, Italy

<sup>4</sup>Institut de Planétologie et d'Astrophysique de Grenoble (IPAG), 120 rue de la Piscine, F-38041 Grenoble, France

<sup>5</sup>LOMC CNRS-UMR6294, Université du Havre, Normandie Université, F-76058 Le Havre, France

<sup>6</sup>Laboratoire Aimé Cotton CNRS-UMR9188, Université Paris-Sud, ENS Cachan, Université Paris-Saclay, F-91405 Orsay, France

Accepted 2019 September 17. Received 2019 September 17; in original form 2019 August 10

## ABSTRACT

Formamide is a potentially important molecule in the context of pre-biotic chemistry, since reactions involving it can lead to precursors of genetic and metabolic molecules. Being abundant in cometary material and in star-forming regions, the formation and destruction routes of interstellar formamide have been the focus of several studies. In this work, we focus on the electron recombination of protonated formamide, an important step of its destruction routes, by performing rigorous *ab initio* calculations of this process. We found that our values are in good agreement with previous qualitative estimates of the global rate coefficients. On the contrary, we propose a substantial revision of the products and branching ratios. Finally, we justify and emphasize the importance of carrying out similar theoretical calculations on the largest possible number of complex species of astrochemical interest.

**Key words:** astrochemistry – molecular data – molecular processes.

## 1 INTRODUCTION

Among the ca. 200 molecules identified in the interstellar medium, formamide ( $\text{NH}_2\text{CHO}$ , also called methanamide and detected for the first time in space by Rubin et al. 1971) has recently attracted particular attention because it gathers together the elements of life (i.e. C, O, and N) arranged in an amide bond ( $-\text{CO}-\text{NH}-$ ) that is the bond that characterizes both peptides (short chains of amino acid monomers) and proteins. In general, an amide bond between two amino acids (also called, in this case, peptide bond) is not easy to form in abiotic environments and the mechanism by which peptide bonds were formed on primitive Earth before the emergence of life is still unknown (Rimola, Sodoupe & Ugliengo 2016, 2019). The detection of formamide and acetamide ( $\text{CH}_3\text{CONH}_2$ ) in the interstellar medium, as well as in comets, suggests that a large supply of simple amides could have been available on primitive Earth because of cometary impacts. In this view, several possible roles of formamide have been proposed in prebiotic chemistry, such as: (1) a solvent favourable to organic synthesis as opposed to water (formamide is a liquid under terrestrial conditions) (Saladino et al. 2012); (2) a precursor of adenine, guanine, cytosine, and uracil, that

is, the four nucleobases of RNA (Ferus et al. 2015); (3) a precursor of amino acids and sugars (Botta et al. 2018).

The presence of formamide in cometary comae and nuclei (Bockelée-Morvan et al. 2000; Biver et al. 2014; Goesmann et al. 2015) indicates that formamide likely existed in relatively large amounts already in the Proto-Solar Nebula, before the final formation of our Solar system. This emphasizes the importance of its search in regions forming solar-like planetary systems. A recent review by Lopez-Sepulcre et al. (2019) shows that formamide is present in high-mass and low-mass star-forming regions (Turner 1989; Bisschop et al. 2007; Isokoski, Bottinelli & Van Dishoeck 2013; Kahane et al. 2013; Mendoza et al. 2014; López-Sepulcre et al. 2015; Taquet et al. 2015; Feng et al. 2016; Ceccarelli et al. 2017; Codella et al. 2017; Oya et al. 2017; Bianchi et al. 2018; Sakai et al. 2018), as well as comets (see above) and other environments including external galaxies (Muller et al. 2013). Clearly, formamide is widely spread in space and the cometary supply can well be the remnant of interstellar synthesis. Its presence in environments with different conditions indicates that there must be an easy formation route, which however remains to be definitely tackled. A plethora of mechanisms have been proposed so far, including: (1) ion–molecule reactions involving protonated or charged species (Quan & Herbst 2007; Redondo, Barrientos & Largo 2013, 2014; Spezia et al. 2016); (2) the neutral–neutral reaction  $\text{NH}_2 + \text{H}_2\text{CO}$  (Barone et al. 2015;

\* E-mail: slavako@ucf.edu

**Table 1.** List of the reactions and their rate coefficients as listed in the KIDA data base. The rate coefficient  $k$  of each reaction is derived from the usual form  $k(T) = \alpha(T/300\text{ K})^\beta$ , where  $\alpha$  is in  $\text{cm}^3\text{ s}^{-1}$  and  $T$  is the gas temperature. All reactions are assumed to be barrier less.

No.	Products	$\alpha$	$\beta$
3(a)	H + NH <sub>2</sub> CHO	$1.5 \times 10^{-7}$	-0.5
3(b)	NH <sub>2</sub> + H <sub>2</sub> CO	$1.5 \times 10^{-7}$	-0.5
3(c)	H + CO + NH <sub>3</sub>	$1.5 \times 10^{-7}$	-0.5
3(d)	H <sub>2</sub> O + H <sub>2</sub> CN	$1.5 \times 10^{-7}$	-0.5
3(e)	H <sub>2</sub> + H <sub>2</sub> + OCN	$1.5 \times 10^{-7}$	-0.5

Skouteris et al. 2017); (3) ice-assisted processes, ranging from hydrogenation of HNCO (Noble et al. 2015; Song & Kästner 2016) or H<sub>2</sub>CO:NO mixtures (Dulieu et al. 2019) to HCO + NH<sub>2</sub> radical recombination (Garrod, Weaver & Herbst 2008; Rimola et al. 2018; Enrique-Romero et al. 2019) as well as processing of various ice mixtures (e.g. NH<sub>3</sub>:CO or H<sub>2</sub>O:HCN) by electron, UV photon, or energetic particle (ions) exposure (Grim et al. 1989; Bernstein et al. 1995; Gerakines, Moore & Hudson 2004; Brucato, Baratta & Strazzulla 2006; Jones, Bennett & Kaiser 2011; Theulé et al. 2013; Dawley, Pirim & Orlando 2014a, b; Henderson & Gudipati 2015; Fedoseev et al. 2016; Kaňuchová et al. 2016; Urso et al. 2017; Ligterink et al. 2018). Whatever the formation mechanism is, however, the main destruction route of gas-phase formamide is via proton-transfer reactions with the abundant HCO<sup>+</sup>, H<sub>3</sub><sup>+</sup>, and H<sub>3</sub>O<sup>+</sup> ions (in warm regions where gaseous water is abundant), with the formation of protonated formamide according to



and so on.

Given the high proton affinity of formamide (822.2 kJ mol<sup>-1</sup>; Hunter & Lias 1998), the most probable fate of its protonated form in the interstellar medium is its recombination with free electrons. From previous experimental evidence on similar species (Geppert & Larsson 2008), we expect that the electron-ion recombination will be of a dissociative kind. Therefore, the proton transfer reactions followed by electron recombination will be main destruction processes of neutral formamide and, presumably, of its amide bond.

The literature search reveals that neither experimental nor theoretical data are available on the dissociative electron recombination reaction of protonated formamide. The KIDA data base includes for the NH<sub>2</sub>CHOH<sup>+</sup> + e<sup>-</sup> reaction guessed values for the overall rate coefficient and product branching ratio given in Table 1. In the absence of experimental or theoretical information, all the channels have been considered to have the same yield. If this is true, only 20 per cent of protonated formamide goes back to neutral formamide. In all other guessed channels, the amide bond is destroyed. Overall, the overall value of  $\alpha$  is  $7.5 \times 10^{-7} \text{ cm}^3 \text{ s}^{-1}$ .

Considering that the destruction routes are as important as the formation routes to correctly predict the molecular abundances in astrochemical models, in this paper we present the first study dedicated to the dissociative recombination (DR) of protonated formamide. In particular, we have performed theoretical calculations to provide an upper limit for the total rate coefficient. The approach is the same as that successfully used to characterize the DR of protonated methanimine, another N-containing species abundant

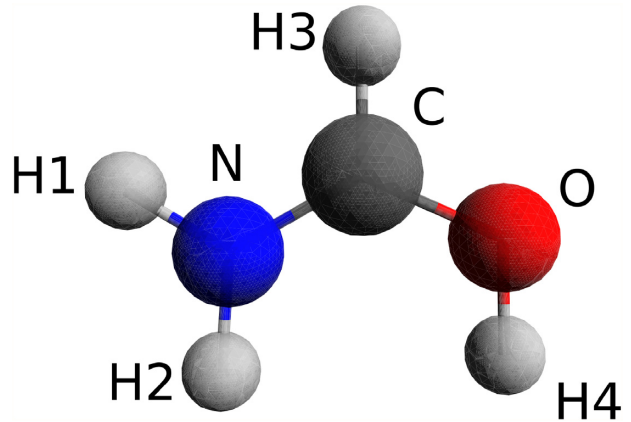


**Figure 1.** Equilibrium configuration of NH<sub>2</sub>CHOH<sup>+</sup>.

**Table 2.** Bond lengths (Å) and angles (°) at the equilibrium geometry of NH<sub>2</sub>CHOH<sup>+</sup>.

N–H1	0.998	N–H2	0.998	N–C	1.285
C–H3	1.074	C–O	1.289	O–H4	0.976
∠H1NH2	117.1	∠H1NC	119.6	∠H3CN	119.6
∠OCN	126.4	∠COH4	114.5		

**Table 3.** Harmonic frequencies of NH<sub>2</sub>CHOH<sup>+</sup> in cm<sup>-1</sup> (10<sup>-3</sup> hartree).

$\omega_1$ (A')	592.45 (2.699)	$\omega_9$ (A')	1516.4 (6.909)
$\omega_2$ (A'')	639.24 (2.913)	$\omega_{10}$ (A')	1730.7 (7.886)
$\omega_3$ (A'')	728.04 (3.317)	$\omega_{11}$ (A')	1858.31 (8.467)
$\omega_4$ (A'')	784.21 (3.573)	$\omega_{12}$ (A')	3370.71 (15.36)
$\omega_5$ (A')	1134.99 (5.171)	$\omega_{13}$ (A')	3672.67 (16.73)
$\omega_6$ (A'')	1204.85 (5.490)	$\omega_{14}$ (A')	3737.39 (17.03)
$\omega_7$ (A')	1231.79 (5.612)	$\omega_{15}$ (A')	3852.28 (17.55)
$\omega_8$ (A')	1473.97 (6.716)		

in extraterrestrial environments (Yuen et al. 2019). Protonation of formamide can occur in two positions: on the lone pairs of oxygen or on that of nitrogen atoms, respectively. In this contribution, we have only considered the protonation on the oxygen atom (see Fig. 1), which is the most stable conformer (Lin et al. 1994). The implications of the present calculations in the chemistry of interstellar formamide will also be addressed.

## 2 THEORETICAL APPROACH

The electronic structure and the vibrational frequencies of NH<sub>2</sub>CHOH<sup>+</sup> are calculated using the MOLPRO suite (Werner et al. 2008). The basis set cc-pVTZ is used for all atoms. The electronic energy is obtained using the complete active space (CAS) self-consistent field method. The first 8  $a'$  orbitals are frozen in the calculation, while the CAS has 5  $a'$  and 3  $a''$  orbitals. NH<sub>2</sub>CHOH<sup>+</sup> has 24 electrons, such that it has a closed-shell ground state configuration  $^1A'$ . At the equilibrium configuration, it possesses C<sub>s</sub> point group symmetry. Fig. 1 displays the equilibrium configuration of NH<sub>2</sub>CHOH<sup>+</sup>, and Table 2 provides details about the configuration. The normal mode frequencies are given in Table 3. Fig. 2 shows the normal displacements for each mode. The modes  $\omega_2$ ,  $\omega_3$ ,  $\omega_4$ , and  $\omega_6$  brake the planar symmetry of the molecule.

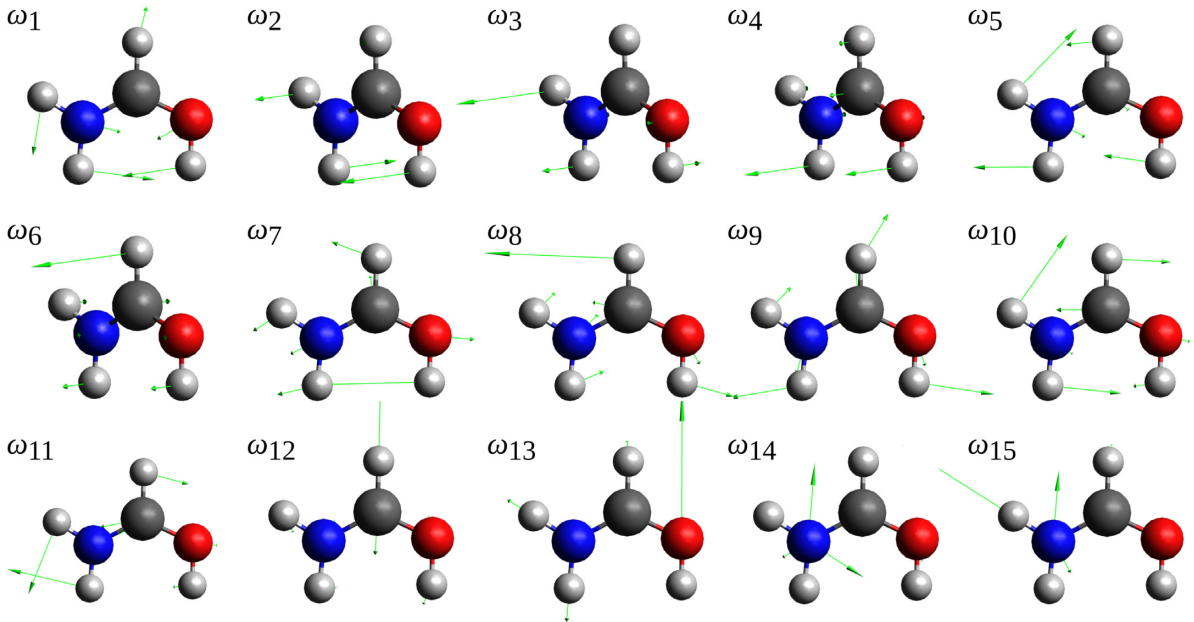


**Figure 2.** Normal modes of  $\text{NH}_2\text{CHOH}^+$ . The colour coding for atoms is the same as in Fig. 1. The arrows indicate the direction and magnitude of displacements for each mode. Note that arrowheads are not shown for the displacements of relatively large magnitudes. For the  $\omega_2$ ,  $\omega_3$ ,  $\omega_4$ , and  $\omega_6$  modes the displacements are pointing out of the plane of the molecule.

Using the QUANTEMOL-N suite (Tennyson et al. 2007), we performed electron-scattering calculations for the  $\text{NH}_2\text{CHOH}^+ + e^-$  collisions using slightly smaller basis set cc-pVDZ than in the structure calculation. The same CAS was employed. Three types (models) of scattering calculations were performed in order to assess the uncertainty of the obtained results, as discussed in detail in Section 4. The final calculations were made using the following parameters (Model 1): We freeze 16 electrons in  $1a'$ ,  $2a'$ ,  $3a'$ ,  $4a'$ ,  $5a'$ ,  $6a'$ ,  $7a'$ , and  $8a'$  core orbitals, while the remaining 8 electrons are kept free in the active space of  $9a'$ ,  $10a'$ ,  $11a'$ ,  $12a'$ ,  $13a'$ ,  $1a''$ ,  $2a''$ , and  $3a''$  molecular orbitals. A total of six electronic excited target states are represented by 900 configuration state functions (CSFs) for the ground state. All the generated states up to 11 eV were retained in the final close-coupling calculation. Due to the large size of the target, the  $R$ -matrix radius is set to be 14 bohr.

Fig. 3 shows the eigenphases sums of the  $\text{NH}_2\text{CHOH}^+ + e^-$  system for  $A'$  and  $A''$  irreducible representations at the equilibrium geometry. The eigenphases sums are smooth functions of energy below 3.2 eV, such that excitation of the doubly excited electronic states can be neglected below that energy. Therefore, one can employ the scattering matrix approach (Fonseca dos Santos et al. 2014). Details about this approach can be found in studies by Fonseca dos Santos et al. (2014) and Yuen et al. (2019). In calculations of cross-sections for vibrational excitation and DR we use the same equations as Yuen et al. (2019), except that the number of vibrational degrees of freedom is larger, so that the sum in equation (5) of Yuen et al. (2019) includes 15 terms, not 12.

### 3 RESULTS AND DISCUSSION

The derivatives of  $S$ -matrix in formulas for the DR and VE cross-sections (equations 3–5 of Yuen et al. 2019) with respect to the normal coordinates are obtained using the finite difference method from two values  $q_i = 0.01$  and  $0.1$  of the normal coordinate

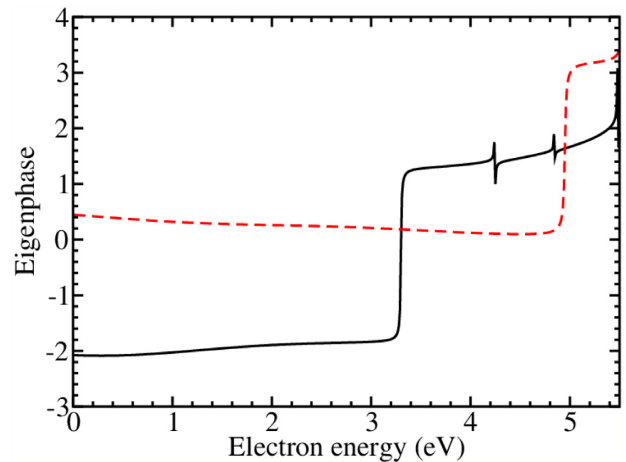


**Figure 3.** Energy-dependence of eigenphases sum of the  $A'$  (solid line) and  $A''$  (dashed line) irreducible representations for the  $\text{NH}_2\text{CHOH}^+ + e^-$  scattering.

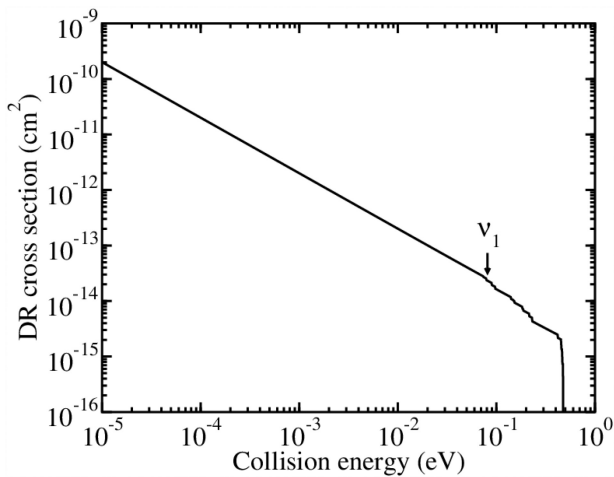
displacements for each mode. The obtained excitation probabilities are smooth with respect to the collision energy, such that they can be fitted with a quadratic function. Table 4 lists the fitted parameters for each normal mode.

Fig. 4 shows the DR cross-section for the target in its vibrationally ground state as a function of collision energy. For energies above 0.1 eV, the cross-section drops in a stepwise manner because the scattering electron excites the vibrational level of the ionic target by one quanta and consequently leaves with a smaller kinetic energy, such that the dissociation step of the process does not occur.

Assuming the collision energy follows the Maxwell–Boltzmann distribution, and the rate coefficients can then be computed analytically and fitted to analytical formulas for a convenient use in plasma models. The analytical formulas are the same in Yuen et al.

**Table 4.** Coefficients from the curve fitting  $P_i = a_i + b_i E + c_i E^2$  ( $E$  in hartree,  $E_h$ ).

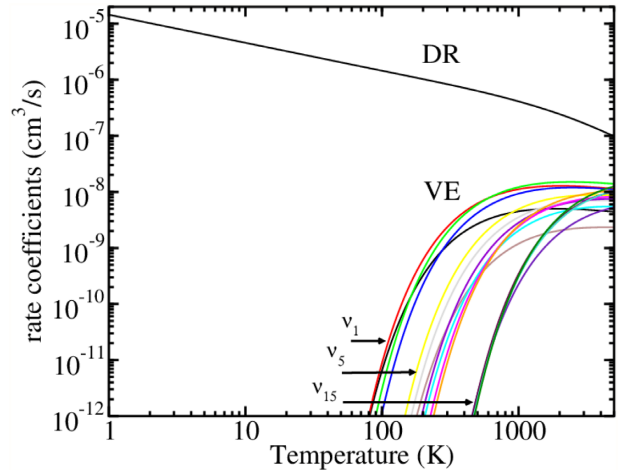
Mode	$a_i$	$b_i (E_h^{-1})$	$c_i (E_h^{-2})$
$P_1$	$3.656 \times 10^{-2}$	$3.506 \times 10^{-1}$	$-4.207 \times 10^{-1}$
$P_2$	$9.769 \times 10^{-2}$	$7.757 \times 10^{-1}$	$-1.495$
$P_3$	$1.189 \times 10^{-1}$	1.223	$-2.999$
$P_4$	$9.909 \times 10^{-2}$	$9.876 \times 10^{-1}$	$-9.634$
$P_5$	$8.761 \times 10^{-2}$	$5.924 \times 10^{-1}$	$-3.051$
$P_6$	$2.309 \times 10^{-2}$	$1.691 \times 10^{-1}$	$6.177 \times 10^{-1}$
$P_7$	$6.844 \times 10^{-2}$	$9.466 \times 10^{-1}$	$-9.961$
$P_8$	$7.926 \times 10^{-2}$	$6.925 \times 10^{-1}$	$-7.830 \times 10^{-1}$
$P_9$	$6.229 \times 10^{-2}$	$3.844 \times 10^{-1}$	$-1.823$
$P_{10}$	$9.809 \times 10^{-2}$	$8.238 \times 10^{-1}$	$-9.701$
$P_{11}$	$1.157 \times 10^{-1}$	1.579	$-9.330$
$P_{12}$	$9.310 \times 10^{-2}$	$5.694 \times 10^{-1}$	3.145
$P_{13}$	$2.380 \times 10^{-1}$	$8.356 \times 10^{-1}$	$-1.985 \times 10^1$
$P_{14}$	$2.024 \times 10^{-1}$	2.071	$-1.557 \times 10^1$
$P_{15}$	$2.534 \times 10^{-1}$	2.292	$-1.464 \times 10^1$

**Figure 4.** DR cross-section as a function of the collision energy. For energies above 0.1 eV, several vibrationally excited channels are open. As a result, the DR cross-section decreases in a stepwise manner.

(2019; see equations 6–8 in that reference). The formulas include fitted parameters  $a_i$ ,  $b_i$ , and  $c_i$ , which are given in Table 4. Using the above analytical fits, the parameters of Table 4, and expressing the product  $k_b T$  in atomic units (hartree), the obtained rate coefficients will be expressed in atomic units. To convert the obtained values into the units  $\text{cm}^3 \text{s}^{-1}$ , the above rate coefficients should be multiplied with factor  $6.126 159 \times 10^{-9}$ .

Fig. 5 displays thermally averaged VE and DR rate coefficients as functions of temperature with the ion being initially in its ground vibrational state,  $v_i' = 0$ . For  $T < 400$  K, the DR rate coefficients behave as  $1/\sqrt{T}$ . Since the exponent factor  $\exp(-\hbar\omega_i/k_b T)$  in equation (8) of Yuen et al. (2019) is much smaller than 1, the DR rate coefficient can be approximated as  $8.33 \times 10^{-7} (300/T)^{0.5} \text{cm}^3 \text{s}^{-1}$ . For  $T > 400$  K, the VE rate coefficients increase rapidly reaching values about  $10^{-8} \text{cm}^3 \text{s}^{-1}$ , while the DR rate coefficient decreases faster than  $T^{-1/2}$ .

The theoretical approach presented above allows us to compute the DR cross-section for the indirect process only, when the incident electron is first captured into a Rydberg resonance attached to the vibrationally excited molecular ion (without electronic excitation of the ion): The electron hits the ion, excites it vibrationally, loses

**Figure 5.** DR (dashed line) and VE (solid lines) rate coefficients for the  $\text{NH}_2\text{CHOH}^+$  ion being initially in the ground vibrational state. To avoid overcrowded labelling, labels for only three VE curves are specified. The lines for all VE rates cross the abscissa in the order of increasing number labelling the modes (and increasing energy  $\hbar\omega_i$ ) as in Table 3. For  $T < 400$  K, the DR and VE rate coefficients behave as  $T^{-1/2}$  and  $T^{-1/2} \exp(-\hbar\omega_i/k_b T)$ , respectively.

its kinetic energy, and stays near the ion for some long time, during which the formed neutral molecule can predissociate rather than ionize. This process, usually referred as the indirect DR, is somewhat different from the one, the direct DR, when the incident electron excites the ion electronically, loses its energy, forming a neutral complex and, if the corresponding potential energy surface of that complex (i.e. of that electronic resonance) is repulsive, leads to dissociation along the repulsive surface (Greene & Kokouline 2006; Douguet et al. 2011). For a significant contribution of the direct DR process to the total DR cross-section, the potential energy surface of the resonant state should cross the ionic potential near the position of the equilibrium. The target  $\text{NH}_2\text{CHOH}^+$  ion has a closed electronic shell such the lowest resonance in the  $e^-$ -ion collisional spectrum appears only around 3.2 eV (see Fig. 3). We have performed calculations exploring the region near the equilibrium of the ion and did not find any low-energy resonance. We also found that the energy of that lowest resonance at 3.2 eV (at equilibrium of the ion) moves around  $3.2 \pm 0.3$  eV for geometries where the vibrational wavefunction of the ion is significant. Therefore, the resonance will not cross the ionic potential surface near the equilibrium (in the region, where the ground vibrational function is localized). So, the low-energy DR process proceeds through capturing the electron into a Rydberg state of an excited vibrational level of the ion, i.e. through an indirect DR process.

#### 4 UNCERTAINTY ESTIMATIONS

The theoretical approach presented above has two major sources of uncertainty: Approximation made by the capture model and the parameters in the scattering model. The former uncertainty has been discussed by Yuen et al. (2019) and assumed to be below 20 per cent. The latter uncertainty can be assessed by using different parameters in the model. The results described above were made with parameters specified in Section 2; this is Model 1. In the second calculation, Model 2, the electronic basis was reduced from cc-pVDZ to 6-311G\*. Finally, in a third calculation, Model 3, the CAS in the configuration interaction calculations was reduced

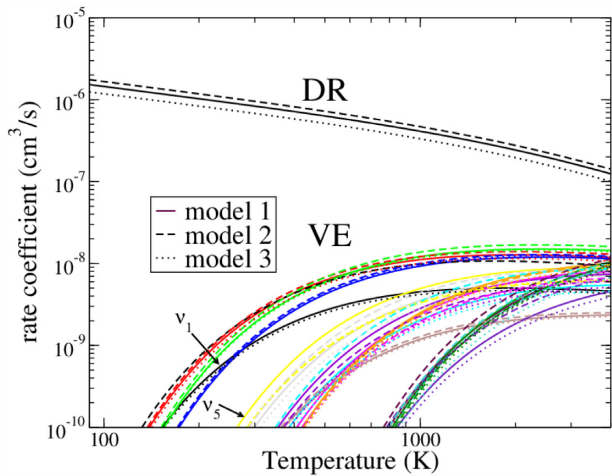


**Figure 6.** DR and VE rate coefficients obtained within three different scattering models – see text. The Model 1 is that described in Section 2. In the Model 2, the basis to represent the electronic wave functions is reduced. In the Model 3, the orbital space in the configuration interaction calculation was reduced with respect to that used in the Model 1. The differences between results obtained in the three models are about 20 per cent.

with respect to Model 1 by 2 spaces. Complete calculations of DR and VE cross-sections and rate coefficients were performed with these changes. The obtained rate coefficients are shown in Fig. 6. The difference between the rate coefficients produced in the three calculations for the DR process is about 15–20 per cent. Therefore, the overall uncertainty of the present theoretical rate coefficients is estimated to be below 40 per cent.

## 5 ASTROPHYSICAL IMPLICATIONS

Since the importance of formamide in the pre-biotic chemistry context (Kahane et al. 2013) was appreciated, several authors have presented specific models focused on explaining the formamide abundance measured in the various environments described in the Section 1 (Garrod et al. 2008; Barone et al. 2015; Codella et al. 2017; Quénard et al. 2017). Those models rely on different formamide formation routes (the gas-phase reaction  $\text{NH}_2 + \text{H}_2\text{CO}$  in Barone et al. (2015), Codella et al. (2017), and a combination of irradiated surface chemistry and gas-phase chemistry in Garrod et al. 2008 and Quénard et al. 2017). On the contrary, the destruction routes are common in all models and are dominated by ion–molecule reactions involving formamide and  $\text{HCO}^+$ ,  $\text{H}_3^+$ ,  $\text{H}_3\text{O}^+$ ,  $\text{He}^+$ , and  $\text{C}^+$ . Moreover, some reactions involving neutral radicals have been invoked, such as the one involving the OH radical (Belloche et al. 2017), but no experimental or theoretical data are available on the rate coefficients for those reactions, which are, anyway, expected to be very slow based on what is known on the reaction  $\text{NH}_2\text{CHO} + \text{H}$  (Haupa, Tarczay & Lee 2019). The proton transfer reactions with  $\text{HCO}^+$  and  $\text{H}_3^+$  dominate the formamide destruction in ‘standard’ conditions, while that with  $\text{H}_3\text{O}^+$  is a dominant formamide sink in the water-rich gas. Instead, the reactions involving  $\text{He}^+$  and  $\text{C}^+$  ions, which provide in general a smaller contribution to the formamide destruction, proceed via charge transfer and lead to a significant fragmentation of the ionized formamide, especially in the case of  $\text{He}^+$  collisions because of the large amount of energy released in the process (see for instance, the article by Ascenzi et al. 2019 for the case of similar molecules). In summary, even though

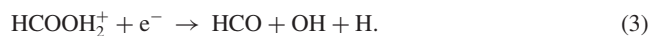
**Table 5.** List of the reactions and their new recommended rate coefficients obtained in this work (see text). We suggest reactions 3b, 3c, 3d, and 3e of Table 1 to be dropped. The rate coefficient  $k$  of each reaction is derived from the usual form  $k(T) = \alpha/\sqrt{(T/300)}$ , where  $\alpha$  is in  $\text{cm}^{-3} \text{s}^{-1}$  and  $T$  is the gas temperature in K (with  $\beta = -0.5$  for all reactions if one uses the standard fit formula given in Table 1). All reactions are assumed to be barrierless.

No.	Products	$\alpha$
3a	$\text{NH}_2\text{CHO} + \text{H}$	$1.2 \times 10^{-7}$
3f	$\text{HCO} + \text{NH}_2 + \text{H}$	$7.1 \times 10^{-7}$

proton transfer processes can lead to fragmentation,  $\text{NH}_2\text{CHOH}^+$  is expected to be also an important by-product in the main destruction route of formamide.

As already mentioned in the Section 1, the most probable fate of protonated formamide will be its recombination with interstellar free electrons. The global electron–ion recombination rate coefficient assumed in the KIDA data base, and used in all the models cited above, is given by  $k(T) = 7.5 \times 10^{-7} (T/300)^{-0.5} \text{cm}^3 \text{s}^{-1}$ , and very nicely compares with the value calculated in this work, which is larger by only 10 per cent, contrarily to other similar cases such as the one of protonated methanimine ( $\text{CH}_2\text{NH}_2^+$ ) where the guessed values substantially differ (Yuen et al. 2019). Our recommendation is to update the data bases for astrochemical modelling with the present value of  $8.33 \times 10^{-7} (T/300)^{-0.5} \text{cm}^3 \text{s}^{-1}$ , which is the result of rigorous calculations rather than an assumed value.

Concerning the branching ratios, our method is not yet able to determine the yield in the different exit channels and, therefore, an experimental determination, such as those achieved by using the heavy ion storage ring CRYRING (Geppert & Larsson 2008), is required. We note, however, that it is highly improbable that all the channels mentioned in the KIDA data base have the same yield. It can be instructive to compare the case of protonated formamide with that of protonated formic acid ( $\text{HCOOH}$ ), as they are isoelectronic species. The DR of protonated formic acid has been experimentally investigated by Vigren et al. (2010). Their experimental thermal rate coefficient was determined to be  $k(T) = 8.4 \times 10^{-7} (T/300)^{-0.78} \text{cm}^3 \text{s}^{-1}$  for electron temperatures between 10 and 1000 K, that is a value quite similar to the one derived here, even though with a temperature dependence slightly steeper. Even closer appear to be the values of the experimental cross-sections as a function of the electron energy (cf. fig. 1 of the paper by Vigren et al. 2010 and that reported in fig. 4 of this manuscript). These latter authors have been able to obtain partial information on the product branching ratio, according to which only 13 per cent of the products retain the skeleton of the heavy atoms (O–C–O in that case). In the modelling of the TMC-1 cold cloud, therefore, they introduced another channel which accounts for the remaining 87 per cent



Reasoning by analogy, we propose that 15 per cent of the protonated formamide electron recombination leads to  $\text{NH}_2\text{CHO} + \text{H}$  and the remaining 85 per cent to  $\text{HCO} + \text{NH}_2 + \text{H}$ . Accordingly, we suggest to substitute the rate coefficients to be used in astrochemical models with those listed in Table 5.

The new chemical scheme implies a significant recirculation of  $\text{NH}_2$ , which is the bottle neck precursor of the gas-phase formation route in the Barone et al. (2015) and Codella et al. (2017) models.

Obviously, an experimental determination only will solve the issue of the branching ratios once for all.

## 6 CONCLUSIONS

We presented the first ever rigorous *ab initio* calculations of the cross-section and rate coefficient for the dissociative electron recombination of protonated formamide, the major species resulting from the most important destruction routes of formamide in standard molecular regions. Data on the electron-induced vibrational transitions of the same cation, useful for a detailed modelling of its kinetics, are also reported.

We found that the overall rate coefficient is substantially similar to previous qualitative estimates given in the KIDA data base, which is used as a reference for astrochemical models: our new values are about 10 per cent larger. Based on the similarity with the isoelectronic protonated formic acid, we have partitioned the global rate coefficient into two channels, of which one leads back to neutral formamide and the other (major) one to the amidogen radical (NH<sub>2</sub>), which is a potential precursor of formamide in the gas-phase.

We recommend to include the new values in the astrochemical data bases, waiting for new experimental or further theoretical approaches resulting in the improvement of the predictivity of astrochemical models. We also plan to extend the same kind of investigation to other crucial species.

## ACKNOWLEDGEMENTS

This work was supported by the National Science Foundation Grant No. PHY-1806915, the Chateaubriand Fellowship and the Thomas Jefferson Fund of the Office for Science and Technology of the Embassy of France in the United States and the program ‘Accueil des chercheurs étrangers’ of CentraleSupélec. It has also received funding from the European Research Council (ERC) under the European Union’s Horizon 2020 research and innovation program, for the Project ‘The Dawn of Organic Chemistry (DOC)’, grant agreement No. 741002. IFS acknowledges the French Programme National ‘Physique et Chimie du Milieu Interstellaire’ (PCMI) of CNRS/INSU with INC/INP, co-funded by CEA and CNES, the RIN-CO<sub>2</sub>-VIRIDIS and the BIOENGINE projects financed by FEDER and La Région Normandie, and the ANR-MONA project.

## REFERENCES

Ascenzi D., Cernuto A., Balucani N., Tosi P., Ceccarelli C., Martini L. M., Pirani F., 2019, *A&A*, 625, A72  
 Barone V., Latouche C., Skouteris D., Vazart F., Balucani N., Ceccarelli C., Lefloch B., 2015, *MNRAS*, 453, L31  
 Belloche A. et al., 2017, *A&A*, 601, A49  
 Bernstein M. P., Sandford S. A., Allamandola L. J., Chang S., Scharberg M. A., 1995, *ApJ*, 454, 327  
 Bianchi E. et al., 2018, *MNRAS*, 483, 1850  
 Bisschop S. E., Jørgensen J. K., van Dishoeck E. F., de Wachter E. B. M., 2007, *A&A*, 465, 913  
 Biver N. et al., 2014, *A&A*, 566, L5  
 Bockelée-Morvan D. et al., 2000, *A&A*, 353, 1101  
 Botta L. et al., 2018, *Adv. Space Res.*, 62, 2372  
 Brucato J. R., Baratta G. A., Strazzulla G., 2006, *A&A*, 455, 395  
 Ceccarelli C. et al., 2017, *ApJ*, 850, 176  
 Codella C. et al., 2017, *A&A*, 605, L3  
 Dawley M. M., Pirim C., Orlando T. M., 2014a, *J. Phys. Chem. A*, 118, 1220

Dawley M. M., Pirim C., Orlando T. M., 2014b, *J. Phys. Chem. A*, 118, 1228  
 Douguet N., Orel A., Mikhailov I., Schneider I. F., Greene C. H., Kokoouline V., 2011, *J. Phys.: Conf. Series*, 300, 012015  
 Dulieu F., Nguyen T., Congiu E., Baouche S., Taquet V., 2019, *MNRAS*, 484, L119  
 Enrique-Romero J., Rimola A., Ceccarelli C., Ugliengo P., Balucani N., Skouteris D., 2019, *ACS Earth Space Chem.*, in press  
 Fedoseev G., Chuang K.-J., van Dishoeck E. F., Ioppolo S., Linnartz H., 2016, *MNRAS*, 460, 4297  
 Feng S., Beuther H., Semenov D., Henning T., Linz H., Mills E. A. C., Teague R., 2016, *A&A*, 593, A46  
 Ferus M., Nesvorný D., Sponer J., Kubelik P., Michalcikova R., Shestivska V., Sponer J. E., Civis S., 2015, *Proc. Natl. Acad. Sci. USA*, 112, 657  
 Fonseca dos Santos S., Douguet N., Kokoouline V., Orel A. E., 2014, *J. Chem. Phys.*, 140, 164308  
 Garrod R. T., Weaver S. L. W., Herbst E., 2008, *ApJ*, 682, 283  
 Geppert W. D., Larsson M., 2008, *Mol. Phys.*, 106, 2199  
 Gerakines P., Moore M., Hudson R., 2004, *Icarus*, 170, 202  
 Goesmann F. et al., 2015, *Science*, 349, aa0689  
 Greene C. H., Kokoouline V., 2006, *Phil. Trans. Royal Soc. A*, 364, 2965  
 Grim R. J. A., Greenberg J. M., de Groot M. S., Baas F., Schutte W. A., Schmitt B., 1989, *A&AS*, 78, 161  
 Haupa K. A., Tarczay G., Lee Y.-P., 2019, *J. Am. Chem. Soc.*, 141, 11614  
 Henderson B. L., Gudipati M. S., 2015, *ApJ*, 800, 66  
 Hunter E. P. L., Lias S. G., 1998, *J. Phys. Chem. Ref. Data*, 27, 413  
 Isokoski K., Bottinelli S., van Dishoeck E. F., 2013, *A&A*, 554, A100  
 Jones B. M., Bennett C. J., Kaiser R. I., 2011, *ApJ*, 734, 78  
 Kahane C., Ceccarelli C., Faure A., Caux E., 2013, *ApJ*, 763, L38  
 Kaňuchová Z., Urso R., Baratta G., Brucato J., Palumbo M., Strazzulla G., 2016, *A&A*, 585, A155  
 Ligerink N., Terwisscha van Scheltinga J., Taquet V., Jørgensen J., Cazaux S., van Dishoeck E., Linnartz H., 2018, *MNRAS*, 480, 3628  
 Lin H.-Y., Ridge D. P., Uggerud E., Vulpus T., 1994, *J. Am. Chem. Soc.*, 116, 2996  
 López-Sepulcre A. et al., 2015, *MNRAS*, 449, 2438  
 López-Sepulcre A., Balucani N., Ceccarelli C., Codella C., Dulieu F., Theule P., 2019, *ACS Earth Space Chem.*, in press  
 Mendoza E., Lefloch B., López-Sepulcre A., Ceccarelli C., Codella C., Boechat-Roberly H., Bachiller R., 2014, *MNRAS*, 445, 151  
 Muller S. et al., 2013, *A&A*, 551, A109  
 Noble J. A. et al., 2015, *A&A*, 576, A91  
 Oya Y. et al., 2017, *ApJ*, 837, 174  
 Quan D., Herbst E., 2007, *A&A*, 474, 521  
 Quénard D., Jiménez-Serra I., Viti S., Holdship J., Coutens A., 2017, *MNRAS*, 474, 2796  
 Redondo P., Barrientos C., Largo A., 2013, *ApJ*, 780, 181  
 Redondo P., Barrientos C., Largo A., 2014, *ApJ*, 793, 32  
 Rimola A., Sodupe M., Ugliengo P., 2016, *JPC*, 120, 24817  
 Rimola A., Skouteris D., Balucani N., Ceccarelli C., Enrique-Romero J., Taquet V., Ugliengo P., 2018, *ACS Earth Space Chem.*, 2, 720  
 Rimola A., Sodupe M., Ugliengo P., 2019, *Life*, 9, 10  
 Rubin R. H., Swenson G. W. Jr, Benson R. C., Tigelaar H. L., Flygare W., 1971, *ApJ*, 169, L39  
 Sakai T. et al., 2018, *ApJ*, 857, 35  
 Saladino R., Crestini C., Pino S., Costanzo G., Di Mauro E., 2012, *Phys. Life Rev.*, 9, 84  
 Skouteris D., Vazart F., Ceccarelli C., Balucani N., Puzzarini C., Barone V., 2017, *MNRAS*, 468, L1  
 Song L., Kästner J., 2016, *Phys. Chem. Chem. Phys.*, 18, 29278  
 Spezia R., Jeanvoine Y., Hase W. L., Song K., Largo A., 2016, *ApJ*, 826, 107  
 Taquet V., López-Sepulcre A., Ceccarelli C., Neri R., Kahane C., Charnley S. B., 2015, *ApJ*, 804, 81  
 Tennyson J., Brown D. B., Munro J. J., Rozum I., Varambhia H. N., Vinci N., 2007, *J. Phys. Conf. Series*, 86, 012001

Theulé P., Duvernay F., Danger G., Borget F., Bossa J., Vinogradoff V., Mispelaer F., Chiavassa T., 2013, *Adv. Space Res.*, 52, 1567  
Turner B., 1989, *ApJS*, 70, 539  
Urso R. G., Scirè C., Baratta G. A., Brucato J. R., Compagnini G., Kaňuchová Z., Palumbo M. E., Strazzulla G., 2017, *Phys. Chem. Chem. Phys.*, 19, 21759  
Vigren E. et al., 2010, *ApJ*, 709, 1429  
Werner H.-J. et al., 2008, MOLPRO, Version 2008.3, A Package of Ab initio Programs

Yuen C., Ayouz M., Balucani N., Ceccarelli C., Schneider I., Kokoouline V., 2019, *MNRAS*, 484, 659

This paper has been typeset from a  $\text{\TeX}/\text{\LaTeX}$  file prepared by the author.